Journal of Physics: Conference Series

PAPER • OPEN ACCESS

Resistive switching in TiO_2 nanocolumn arrays electrochemically grown

To cite this article: M Marik *et al* 2017 *J. Phys.: Conf. Ser.* **829** 012001

View the article online for updates and enhancements.

Related content

- Effect of oxygen concentration and metal electrode on the resistive switching in MIM capacitors with transition metal oxides
D Spassov, A Paskaleva, K Fröhlich et al.
- Corrigendum: Ga-polar GaN nanocolumn arrays with semipolar faceted tips (2013 *New J. Phys.* **15** 053045)
A Urban, J Malindretos, J-H Klein-Wiele et al.
- Mechanisms of charge transport and resistive switching in composite films of semiconducting polymers with nanoparticles of graphene and graphene oxide
A S Berestennikov and A N Aleshin

IOP ebooks™

Bringing you innovative digital publishing with leading voices to create your essential collection of books in STEM research.

Start exploring the collection - download the first chapter of every title for free.

This content was downloaded from IP address 147.229.6.155 on 04/12/2018 at 08:57

IOP Conf. Series: Journal of Physics: Conf. Series **829** (2017) 012001 doi:10.1088/1742-6596/829/1/012001

Resistive switching in TiO_2 nanocolumn arrays electrochemically grown

M Marik, A Mozalev, J Hubalek and M Bendova

CEITEC – Central European Institute of Technology, Brno University of Technology, Purkynova 123, Brno 61200, Czech Republic

E-mail: marian.marik@ceitec.vutbr.cz

Abstract. Resistive switching in metal oxides, especially in TiO_2, has been intensively investigated for potential application in non-volatile memory microdevices. As one of the working mechanisms, a conducting filament consisting of a substoichiometric oxide phase is created within the oxide layer. With the aim of investigating the filament formation in spatially confined elements, we fabricate arrays of self-ordered TiO_2 nanocolumns by porous-anodic-alumina (PAA)-assisted anodizing, incorporate them into solid-state microdevices, study their electron transport properties, and reveal that this anodizing approach is suitable for growing TiO_2 nanostructures exhibiting resistive switching. The electrical properties and resistive switching behavior are both dependent on the electrolytic formation conditions, influencing the concentration and distribution of oxygen vacancies in the nanocolumn material during the film growth. Therefore, the PAA-assisted TiO_2 nanocolumn arrays can be considered as a platform for investigating various phenomena related to resistive switching in valve metal oxides at the nanoscale.

1. Introduction

Investigation of switching behavior of several metal oxides, which may have their resistance states modulated by voltage applied to or by the current flowing through them, is nowadays a growing research field motivating researchers and engineers to develop high-speed low-power nano-dimensional non-volatile Resistive Random Access Memory (ReRAM) devices. In such devices, a layer of metal oxide is usually sandwiched between two metallic electrodes for obtaining metal/semiconductor/metal structures. TiO_2, among other metal oxides like Ta_2O_5, HfO_2, ZrO_2, ZnO, WO_3, or NiO is one of the most intensively investigated resistive switching materials because of many advantages, such as the versatile fabrication techniques and suitable electrical properties resulting from a wide band gap and high dielectric constant [1,2,3].

A common mechanism of resistive switching in metal oxides is the formation of a thin conducting filament within the oxide layer, based on the field-induced movement of mobile oxygen vacancies [4,5]. A further filament rupture and re-creation at one of the interfaces between the metal oxide and a metal electrode, while applying voltage, is often the underlying phenomenon behind a bipolar resistive switching [5]. The filament is thus composed of a substoichiometric crystalline phase of the metal oxide, a Magnéli phase [6], formed also due to the high temperatures achieved during the local heating [7].

Nanostructuring of TiO_2 to the lateral size being comparable with a filament diameter (~15 nm [6]) may spatially confine the filament formation, leading to phenomena different from those occurring in

Content from this work may be used under the terms of the Creative Commons Attribution 3.0 licence. Any further distribution of this work must maintain attribution to the author(s) and the title of the work, journal citation and DOI.
Published under licence by IOP Publishing Ltd

continuous thin films. This motivated our efforts to incorporate arrays of TiO_2 nanocolumns prepared via the porous-anodic-alumina (PAA)-assisted anodizing [8,9] into a 3-D solid-state microdevice and investigate their electrical transport properties. The advantage is that the sizes of nanocolumns can be well controlled through the anodizing variables. In addition, the specific electrolytic conditions applied during the PAA-assisted film growth may enable tuning stoichiometry of the oxides and thus modification of their electrical behavior. In the present work, we fabricate PAA-assisted TiO_2 nanocolumn arrays, embedded in the anodic alumina matrix, by varying the anodizing conditions. We incorporate the arrays into metal/semiconductor/metal microdevices by electrochemically depositing top gold electrodes and measure their room-temperature current-voltage behavior, revealing the right combination of electrolytic conditions appropriate for the occurrence of bipolar resistive switching in the anodic films.

2. Experimental details

2.1. Fabrication of the TiO_2 arrays

A silicon wafer covered with a 500 nm thick thermal oxide layer was used as a starting substrate. A high quality Al/Ti bilayer (aluminum-on-titanium, 500/300 nm thick) was deposited via ion beam sputtering. The wafer with the deposited metal layers was cut into 10 mm ×15 mm pieces, which were individually processed in a closed two-electrode PTFE cell with a stainless steel counter electrode, exposing a surface area of 28 mm^2. Anodizing and re-anodizing experiments were performed in 0.3 M oxalic acid solution at 10 °C. Anodizing at a constant potential of 40 V led to formation of a PAA matrix having self-ordered nanopores, with nanoprotrusions of TiO_2 within the alumina barrier layer at the bottom of the PAA film having a mean diameter of ~35 nm. Re-anodizing to a higher anodic potential with a sweep rate of 2 $V \cdot s^{-1}$ resulted in relatively longer TiO_2 nanocolumns, while their length was tuned by setting the value of re-anodizing potential to 70, 100, and 130 V (arrays A) [10,9]. In addition, the nanocolumns grown to 100 V were prepared also by re-anodizing with a sweep rate of 0.2 $V \cdot s^{-1}$ (array B-100V). The typical current-time and potential-time transients obtained for the two sample types, re-anodized to 100 V, are shown in figure 1, supported by the schemes of nanoarray structure at the different stages of PAA-assisted film growth. The samples were further modified by annealing at 500 °C in vacuum (10^{-4} Pa).

To form the top contact to the TiO_2 nanocolumns and thus obtain a memory cell, gold was electrochemically deposited onto the column tops within and over the PAA nanopores [11,12]. The size of the top Au electrode was defined by an etch-back photolithography to ~100 μm × 100 μm.

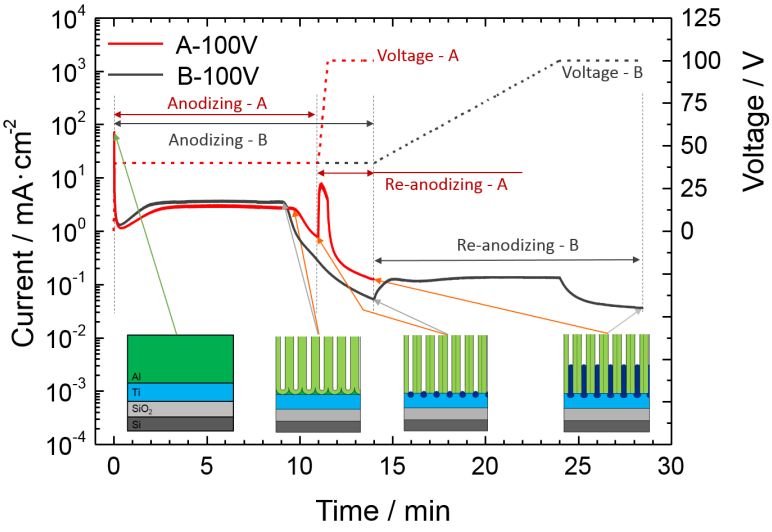

Figure 1. Current-time and potential-time transients recorded during the PAA-assisted anodization of arrays A-100V (red) and B-100V (black). The different regions (anodizing and re-anodizing) are marked and the images show schematically the arrays at the corresponding current or potential changes.

2.2. Characterization

Experimental samples (surfaces and cross-fractures) were observed by scanning electron microscopy (SEM) using a Tescan Mira II at different stages of sample fabrication. The electrical characterization was performed at room temperature using a Keithley 4200 SMU system connected to a CASCADE M150 probe station with magnetic micromanipulators, by recording $I(V)$ curves with a scan rate of 100 $mV \cdot s^{-1}$ from 0 to +5.0, then to −5.0 and back to 0 V in each cycle. To avoid damage of the microcells, the current compliance limit was set to 100 mA. The top Au pad was biased in all $I(V)$ measurements, while the bottom Ti layer, remaining after the PAA-assisted anodizing and being common for all devices prepared on a single chip, was grounded. The measured current and the calculated resistance were related to the projected area of the microcells.

3. Results and discussion

Arrays of TiO_2 nanocolumns are prepared via PAA-assisted anodizing to investigate their electrical properties with the focus on resistive switching application. The anodizing procedure is varied to obtain nanocolumns of variable length (increasing with the re-anodizing potential) and of different stoichiometry (possibly tuned by the potential sweep rate during the re-anodizing). To enable a good electrical contact to each nanocolumn in the array, gold is electrochemically deposited onto the TiO_2 columns, filling the alumina pores and growing over the alumina surface, which is constrained to square-shaped pads of a micrometer size. Typical examples of the devices and their cross fractures are displayed in the SEM images of figure 2, where the different array components can be seen and are schematically shown. A homogeneous filling of the alumina pores, with most of the TiO_2 nanocolumns contacted by gold, is desirable. The pore filling achieved in this study was not worse than 75%.

Typical initial $I(V)$ characteristics of the arrays A (i.e. having the *higher potential sweep rate* during re-anodizing) processed to different final potentials are shown in figure 3a in a logarithmic representation to emphasize the differences between the samples. Each of these arrays, comprising TiO_2 nanocolumns of various lengths, reveals non-linear shape of the corresponding $I(V)$ curve, also showing substantial current drops and jumps for the 70V and 130V arrays and an asymmetric diode-like behavior for the A-100V and A-130V samples. The initial resistance at 0 V ($R_{initial,0V}$) increases with increasing re-anodizing potential, from ~0.25 $\Omega \cdot cm^2$ for sample A-70V to ~7.5 $\Omega \cdot cm^2$ for both A-100V and A-130V arrays. Further $I(V)$ cycling (see figure 3b) shows again non-linear characteristics with an increased current density as compared with the initial state, being asymmetric only for the A-100V and A-130V arrays. The cycling resistance at 0 V ($R_{cycles,0V}$) is thus lower than that in the initial measurement by about ten and two times in case of sample A-70V and samples A-100V and A-130V respectively.

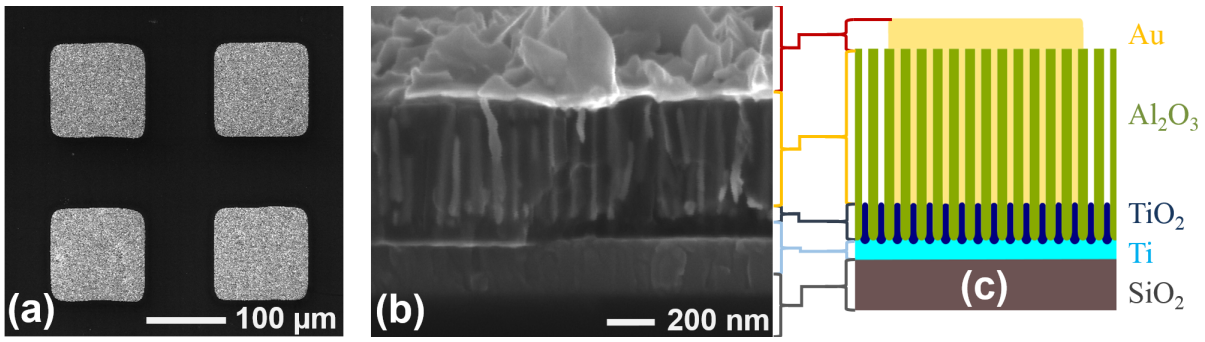

Figure 2. (a) Panoramatic and (b) cross-fractional SEM images of microcells consisting of A-100V nanocolumns. (c) Schematic drawing of the cross-section of a device, explaining the different layers visible in the SEM image of panel (b).

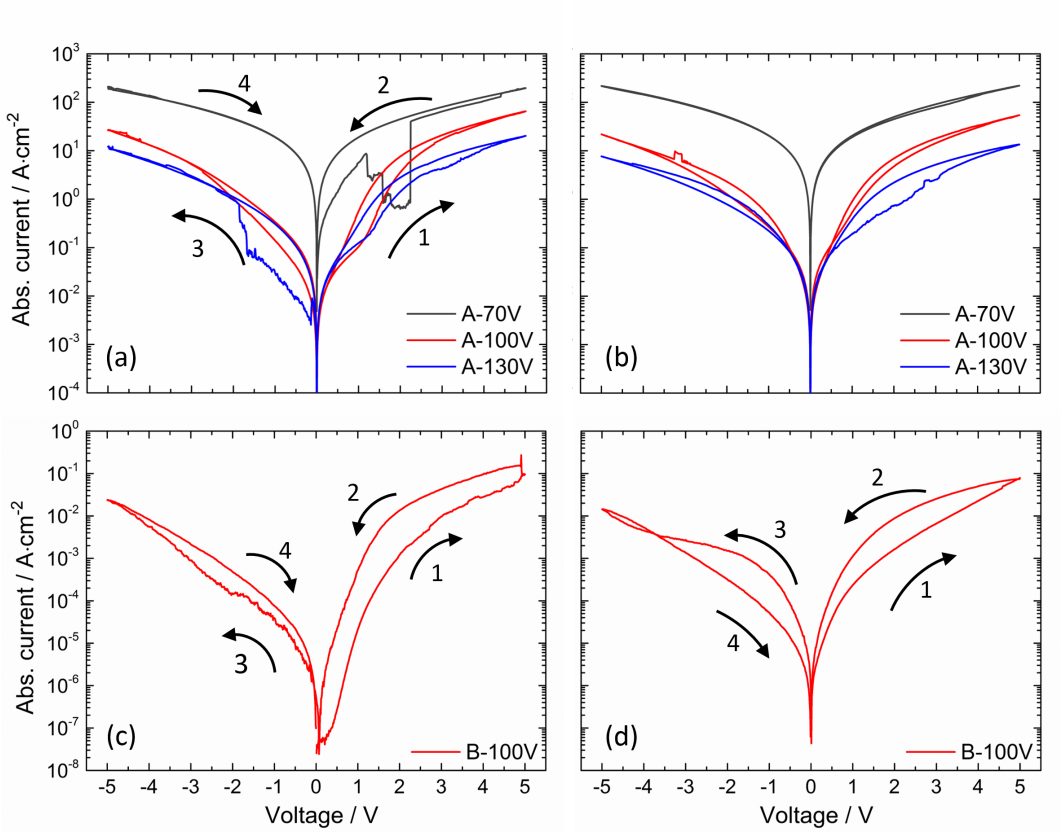

Figure 3. (a,c) The initial and (b,d) further $I(V)$ cycles obtained (a,b) for arrays A (i.e. formed at the higher potential sweep rate during re-anodizing) and (c,d) for arrays B (i.e. formed at the lower potential sweep rate during re-anodizing). The cycling was performed in the order 0 → +5.0 → −5.0 → 0 V without any break in applying voltage, at a scan rate of 100 mV·s^{-1} at room temperature. The top Au electrode was biased while the bottom Ti layer was grounded. The arrows indicate the scan direction.

The electrical characterization of the arrays A therefore does not reveal any resistive switching behavior, for which a substantial decrease of resistance after the initial $I(V)$ cycle accompanied by a presence of high- and low-resistance states (HRS and LRS, respectively) in the following cycles is expected [12]. The observed current jumps and drops in the initial $I(V)$ curves of arrays A (figure 3a) are rather caused by imperfect contacting, and there are no signs of distinguishable HRS and LRS in the following cycles. On the other hand, the resistance increases with the re-anodizing potential, which is in line with the increasing length of the nanocolumns and with their semiconductive nature. In addition, as samples A-100V and A-130V have their initial and consecutive $I(V)$'s similar to each other but different from those of sample A-70V (see the curve shape and symmetry), different conduction mechanisms are expected in these array groups. The oxygen-deficient root structure [13] of A-70V columns in the PAA barrier may prevail in the shorter nanocolumns, whereas a more stoichiometric, i.e. less conducting column body situated over the roots may lead to the diode-like behavior of A-100V and A-130V arrays, possibly with a Schottky barrier created at the Au/TiO_2 interface [12].

To alter the electrical behavior of the PAA-assisted TiO_2 nanocolumns, an array of type B (i.e. having the *lower potential sweep rate* during re-anodizing) was also prepared and electrically characterized. An initial $I(V)$ curve of sample B-100V (figure 3c) shows a non-linear asymmetric behavior with $R_{initial,0V}$ of ~$6 \cdot 10^5$ Ω·cm^2 and a current jump at 5.0 V, leading to a drop in the resistance of about one order of magnitude. The consecutive cycling (figure 3d) reveals also a non-linear

asymmetric $I(V)$ characteristic and, in addition, the presence of HRS and LRS having $R_{cycles,0V}$ of ~$3 \cdot 10^4$ and ~$8 \cdot 10^3$ $\Omega \cdot cm^2$, respectively.

The array B-100V shows therefore signs of bipolar resistive switching. During the initial, forming $I(V)$ cycle, a conducting filament is probably formed within the columns or at one of the interfaces [12]. The switching direction, i.e. the transformation of HRS into LRS, happening at the positive polarization of the top Au electrode, followed by a transition from LRS into HRS at the negative polarization, indicates that the switching interface is the bottom one (TiO_2/Ti) [12]. The absence of abrupt current or resistance change during one of these transitions may indicate synaptic behavior of the array [14], executed in this case by inhomogeneous switching events in the multiple channels present in the array.

Comparing the anodizing conditions during the nanocolumn growth with the electrical behavior of arrays A and B, we see the following relations, summarized schematically in figure 4. The higher potential sweep rate during the re-anodizing (arrays A) leads to the formation of nanocolumns having a relatively low initial resistance (between 0.25 and 8 $\Omega \cdot cm^2$), whereas the lower potential sweep rate (array B) seems to increase the resistance ($6 \cdot 10^5$ $\Omega \cdot cm^2$). This may be explained by a formation of more oxygen-deficient and thus more electrically conducting nanocolumns in the case of the faster sweep rate during the column formation (arrays A) as compared to more stoichiometric oxide formed during the slower sweep rate (arrays B) [15]. Such higher-resistance, more-stoichiometric TiO_2 nanocolumns would be expected to lead to bipolar resistive switching behavior [5], as it is indeed observed in the present study. In addition, the length of the nanocolumns seems to have also an influence on their electrical resistance, possibly due to an inhomogeneous distribution of oxygen vacancies along the nanocolumn material, as manifested in arrays A by the increase in the resistance with increasing nanocolumn length, accompanied by the diode-like $I(V)$ characteristics of the longer A-100V and A-130V nanocolumns. To confirm this mechanism, as well as to elucidate the role of the annealing in vacuum on the concentration and distribution of oxygen vacancies, further analytical and electrical characterization of the arrays is being performed. Additionally, TiO_2 nanocolumn arrays grown at modified electrochemical conditions are currently under investigation; the results to be reported in due course.

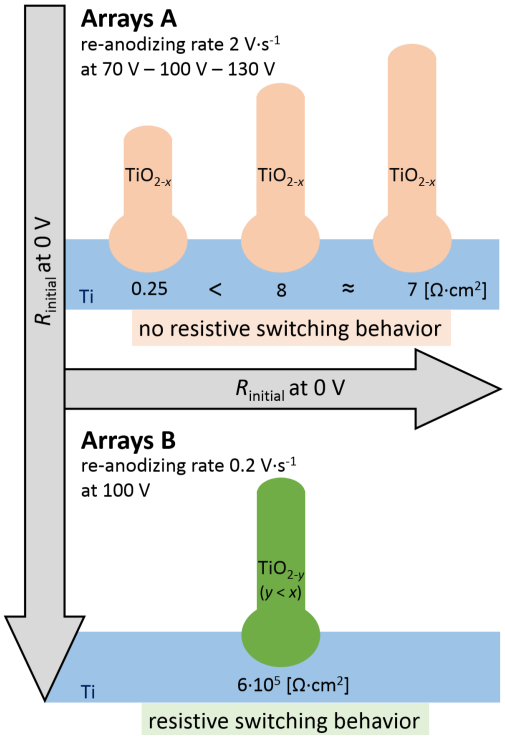

Figure 4. Schematic representations of PAA-assisted-anodized TiO_2 nanocolumns re-anodized to different potentials showing the relations between the anodizing conditions, oxide stoichiometry, and electrical properties. The faster re-anodizing rate (arrays A, upper part) results in a lower $R_{initial,0V}$ and reveals no sign of resistive switching, whereas the slower re-anodizing rate (arrays B, lower part) leads to the formation of more stoichiometric columns having a high $R_{initial,0V}$ and showing the resistive switching.

4. Conclusion

In this study, PAA-assisted well-ordered TiO_2 nanocolumn arrays were prepared and electrically characterized. Two different array types, A and B, grown at modified anodizing conditions, showed significant differences between their electrical and especially resistive switching behavior. Type A arrays, grown at a faster potential sweep rate, revealed lower resistances, increasing with the column length, and showed no sign of resistive switching. On the other hand, the nanocolumns fabricated at a slower potential sweep rate (type B) showed higher initial resistances and revealed a bipolar resistive switching behavior. The behaviors correlate with the oxygen-vacancy distribution established in the nanocolumns during anodic film growth. Thus, the PAA-assisted TiO_2 nanocolumn arrays form a basis for further development of resistive switching microdevices and for investigation of fundamental phenomena like the size-confinement effect in the metal-oxide nanostructures crucial for the filament formation.

Acknowledgements

Research leading to these results was supported in part by the Czech Science Foundation (GA ČR) under the grant no. 15-23005Y and in part by the Ministry of Education, Youth and Sports of the Czech Republic under the project CEITEC 2020 (LQ1601).

References

[1] Vazquez R M, Gispert-Guirado F, Llobet E and Mozalev A 2014 Proceedings of IEEE sensors 2014 (IEEE Service Center, USA) pp 807–810 DOI: 10.1109/ICSENS.2014.6985122
[2] Yang J J, Strukov D B and Stewart D R 2013 *Nat. Nanotechnol.* **8** 13–24
[3] Yang J J, Pickett M D, Li X, Ohlberg D A A, Stewart D R and Williams R S 2008 *Nat. Nanotechnol.* **3** 429–433
[4] Sawa A 2008 *Mater. Today* **11** 28–36
[5] Waser R, Dittmann R, Staikov G and Szot K 2009 *Adv. Mater.* **21** 2632–2663
[6] Kwon D-H, Kim K M, Jang J H, Jeon J M, Lee M H, Kim G H, Li X-S, Park G-S, Lee B, Han S, Kim M and Hwang C S 2010 *Nat. Nanotechnol.* **5** 148–153
[7] Marchewka A, Roesgen B, Skaja K, Du H, Jia C-L, Mayer J, Rana V, Waser R and Menzel S 2016 *Adv. Electron. Mater.* **2** 1500233
[8] Tatarenko N I and Mozalev A M 2001 *Solid-State Electron.* **45** 1009–1016
[9] Sjöström T, Fox N and Su B 2010 *Electrochim. Acta* **56** 203–210
[10] Vázquez R M, Calavia R, Llobet E, Guirado F, Hubálek J and Mozalev A 2012 *Procedia Eng.* **47** 833–836
[11] Mozalev A, Bendova M, Vazquez R M, Pytlicek Z, Llobet E and Hubalek J 2016 *Sens. Actuators, B* **229** 587–598
[12] Bendova M, Hubalek J and Mozalev A 2016 *Adv. Mater. Interfaces* **3** 1600512
[13] Chang Y-H, Lin H-W and Chen C 2012 *J. Electrochem. Soc.* **159** D512–D517
[14] Chang T, Jo S-H, Kim K-H, Sheridan P, Gaba S and Lu W 2011 *Appl. Phys. A* **102** 857–863
[15] Knörnschild G, Poznyak A A, Karoza A G and Mozalev A 2015 *Surf. Coat. Technol.* **275** 17–25